

Vibrational Quantum-State-Controlled Reactivity in the $O_2^+ + C_3H_4$ Reaction

C. Zagorec-Marks,^{*,†,‡} G. S. Kocheril,^{¶,‡} T. Kieft,^{¶,‡} O. A. Krohn,^{§,¶,‡} C. Martí,[§]
T. P. Softley,^{||} J. Zádor,[§] and H. J. Lewandowski^{*,¶,‡}

[†]*Department of Physics, University of Colorado, Boulder, CO 80309, USA*

[‡]*JILA, National Institute of Standards and Technology and the University of Colorado,
Boulder, CO 80309, USA.*

[¶]*Department of Physics, University of Colorado, Boulder, CO 80309*

[§]*Combustion Research Facility, Sandia National Laboratories, Livermore, CA 94550, USA*

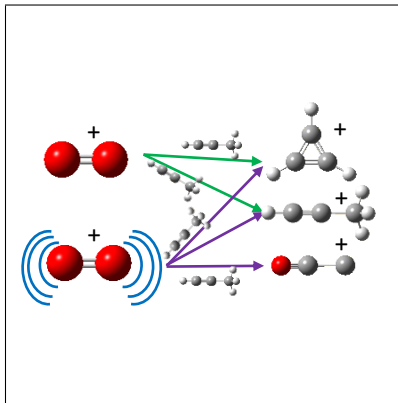
^{||}*School of Chemistry, University of Birmingham, Edgbaston, B15 2TT, UK*

E-mail: chase.zagorec-marks@colorado.edu; lewando@colorado.edu

Abstract

Quantum-state-controlled reactivity is a long-standing goal in the field of physical chemistry. In this work, we explore the vibrational-state-dependent behavior of the ion-molecule reaction between O_2^+ in distinct vibrational states and two isomers of C_3H_4 , allene ($H_2C_3H_2$) and propyne (H_3C_3H). While most products are formed regardless of the vibrational state of O_2^+ , the branching ratios are influenced by vibrational excitation, and a new product, C_2O^+ , appears exclusively in the excited-state reactions. This selective formation of C_2O^+ demonstrates that vibrational excitation can effectively activate a reaction pathway, providing direct evidence of quantum-state control in reactivity. These results represent an important step towards the goal of quantum-state-controlled chemistry in molecular systems.

TOC Graphic



Understanding the role of individual quantum states on reactivity is a critical component to developing control of chemical reaction processes, which is an often-stated goal for the physical chemistry community.¹ Original endeavors to achieve this goal investigated the effects of individual quantum states in atom-diatom reactions and resulted in the development of Polanyi's rules.²⁻⁵ With these rules, Polanyi suggested that not all forms of energy (vibrational, translational, etc.) are equivalent in determining the progression of a reaction. Specifically, as observed in these early studies, translational energy facilitated an atom-diatom reaction's progression through an early barrier (i.e., a barrier located along the approach coordinate of reaction); whereas, vibrational energy facilitated progression through a late barrier (i.e., a barrier located along the separation coordinate). Additionally, it was seen that the energy distribution of the reaction products depended on the position of the barrier, with an early barrier promoting greater partitioning of energy into the products' vibrational modes and a late barrier promoting greater partitioning into the products' translational energy.

Additional experimental support for Polanyi's rules was provided with the advent of lasers. This development renewed interest in state-dependent chemistry, as quantum states of reactants could be directly populated in atom-diatom reaction systems.⁶ However, as studies expanded to polyatomic systems, it was found that Polanyi's rules were often not sufficient, particularly for ion-molecule reactions in which submerged barriers are commonly present.⁷⁻¹² More recent theoretical efforts have extended Polanyi's rules to be more applicable to polyatomic reactions through the use of quasi-classical trajectory simulations, quantum dynamics calculations, and sudden vector projection models.¹³⁻¹⁹

Although there has been a significant amount of theoretical progress in exploring state-dependent reactivity,^{1-5,13-19} there has been less experimental progress.^{18,20-29} This is due to the experimental difficulty in preparing reactants in a pure quantum state and ensuring that these reactants do not decay to their ground state or, in the case of polyatomic molecules, disperse the excitation energy via intramolecular vibrational redistribution (IVR) prior to

the reaction.

Ion–molecule reactions are especially well suited for studies of quantum-state–controlled chemistry, since they are typically exothermic and barrierless. Such reactions proceed rapidly ($k \sim 10^{-9}, \text{cm}^3 \text{ s}^{-1}$)³⁰ and often occur too quickly for significant redistribution of energy among different internal states. In particular, homonuclear diatomic ions are ideal for studying vibrational-state-dependent reactivity because their lack of an electric dipole moment can result in long-lived, excited vibrational states, and they are immune to IVR by having only one fundamental vibrational mode.^{31,32} O_2^+ is an apt candidate for such studies, as the vibrational lifetime of the $X^2\Pi_g$ state has been calculated to be as long as 5.7×10^5 s for the $v = 30$ vibrational mode, with even longer lifetimes predicted for lower-lying states, as their decay proceeds solely through quadrupole emission.³³

Previously, we investigated reactions of O_2^+ in the $X^2\Pi_g$ vibrationally excited states ($v = 2,3$) with the C_3H_4 isomers, allene ($\text{H}_2\text{C}_3\text{H}_2$) and propyne ($\text{H}_3\text{C}_3\text{H}$), to elucidate the influence of isomeric structure on reactivity. These studies were conducted as a follow-up to our earlier work on the reactions of C_2H_2^+ with these C_3H_4 isomers.^{34,35} While many of the products observed in the original study with C_2H_2^+ were also detected in the reaction with O_2^+ (the primary products $\text{c-C}_3\text{H}_3^+$ and C_3H_4^+ , and the secondary products C_6H_5^+ and C_6H_7^+), there were also distinct results.³⁶ Specifically, it was observed that, contrary to prior studies, both C_3H_4 isomers formed a covalently-bound reaction complex with O_2^+ and the minor product, which was suggestive of complex formation and had a mass-to-charge ratio (m/z) of 40 m/z , was found to be non-reactive to C_3H_4 , which was evidence that it may be a product other than C_3H_4^+ . C_2O^+ was previously proposed as the identity of this non-reactive 40 m/z based on the lack of reactivity and the reaction’s atomic composition. The possible production of C_2O^+ in that study, in addition to the knowledge that O_2^+ had been formed in a mixture of vibrationally excited states ($v = 2,3$), encouraged our further exploration into how vibrational excitation may influence this reaction. Here, we explored the effects of vibrational excitation of O_2^+ on the ion–molecule reactions, shown below, between O_2^+ and

the C₃H₄ isomers.



We found that the vibrational state of O₂⁺ governs the formation of the non-reacting 40 *m/z* product, which is identified as C₂O⁺, and this product is produced only upon vibrational excitation of O₂⁺ despite the presence of a barrierless formation pathway even in the ground state. Thus, we have been able to demonstrate how reactions of O₂⁺ in different vibrational states can impact the dynamics and ultimately the reaction products.

The remainder of this letter is organized as follows. First, a brief description of the experimental apparatus is provided so that the results can be more readily interpreted. This is followed by a short discussion of previous experimental results for the reactions of O₂⁺,³⁶ in the *v* = (2,3) excited vibrational states, with both C₃H₄ isomers, allene (H₂C₃H₂) and propyne (H₃C₃H). Next, new data for the reactions of O₂⁺, in the ground vibrational state, with both C₃H₄ isomers is presented and discussed. Finally, these results are compared, thereby demonstrating how O₂⁺'s vibrational state affects the progression of these reactions.

The experimental apparatus is summarized here (with full details in the Methods section) to provide context for the results. The experiment uses atomic-physics techniques to achieve single-collision conditions and ion translational temperatures below 10 K, where temperature here refers to a spread in energy and is not representative of a true temperature of a Maxwell-Boltzmann distribution.

To achieve these conditions, laser-cooled Ca⁺ ions are confined in a linear, quadrupole ion trap within an ultra-high-vacuum chamber, forming a pseudo-crystalline structure known as a Coulomb crystal, which sympathetically cools co-trapped molecular ions through Coulomb interactions. The O₂⁺ ions are created by two separate (2+1) resonance enhanced multi-photon ionization (REMPI) schemes, which create ions predominantly in the ground state

($\sim 91\%$ in ground state) or a mixture of excited vibrational states ($v = 2$ and 3 , $\sim 68\%$ and $\sim 28\%$ of ions, respectively).^{37–40} Because the ions are separated by $\sim 10 \mu\text{m}$, this sympathetic cooling acts on only translational motion and does not impact vibrational-state populations. Combined with the ultra-high-vacuum environment, which leads to a low rate ($< 1 \text{ Hz}$) of background gas collisions, this ensures that O_2^+ remains in its initial vibrational state until a reactive collision occurs. The vacuum conditions further preclude termolecular processes, so internal energy in reaction complexes can dissipate only through bimolecular dissociation or radiative decay.

Reactions are initiated by introducing neutral C_3H_4 into the vacuum system at pressures that result in collision rates on the order of $\sim 1 \text{ Hz}$. After C_3H_4 is admitted for a set amount of time, the trap contents (which include all charged reactants and products) are extracted into a time-of-flight mass spectrometer. Reaction curves are obtained by repeating this procedure with a range of reaction times.

We first consider previous results where vibrationally excited $\text{O}_2^+(v = 2,3)$ reacted with two C_3H_4 isomers.³⁶ The reaction curves from that work are shown in Fig. 1. In these reactions, we observed that the primary product formed was $c\text{-C}_3\text{H}_3^+$ (blue points), which accounted for $\sim 73\%$ (~ 130 ions) of all products in the reaction of O_2^+ with allene and $\sim 62\%$ (~ 110 ions) of all products in the reaction of O_2^+ with propyne.

Because $c\text{-C}_3\text{H}_3^+$ has been observed to be far less reactive than its linear counterpart with a variety of molecules and it has a $m/z=39$,^{34,41–44} we assigned this structure to the observed 39 m/z product. In addition to $c\text{-C}_3\text{H}_3^+$, we indirectly observed another product channel at 40 m/z (orange points), which accounted for $\sim 17\%$ (~ 30 ions) of all products in the reaction of O_2^+ with allene and $\sim 30\%$ (~ 70 ions) of all products in the reaction of O_2^+ with propyne. Although we would have preferred a direct measurement of this product channel, the presence of Ca^+ (~ 700 ions) at the same mass led to a large intrinsic uncertainty in the measurement of this much smaller number of product ions. This uncertainty was mostly due to the natural shot-to-shot variations in the loading of Ca ions into the trap (± 50 ions),

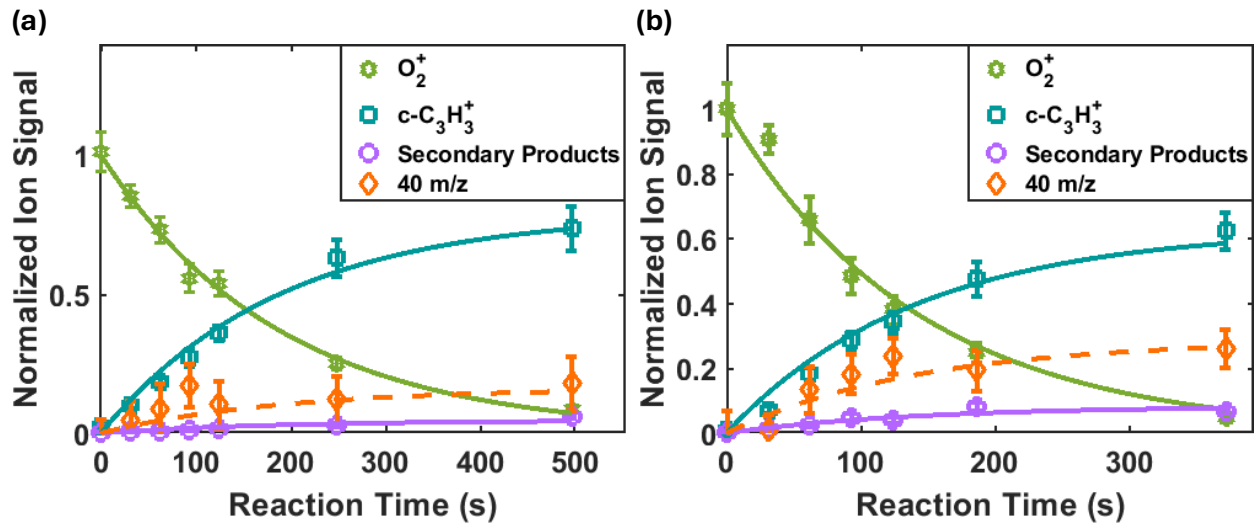


Figure 1: Reaction curves for (a) $\text{O}_2^+(v = 2,3) + \text{H}_2\text{C}_3\text{H}_2$ (allene) and (b) $\text{H}_3\text{C}_3\text{H}$ (propyne) reaction series. As the O_2^+ signal decreases (green), immediate growth is observed in the 39 m/z (teal) and 40 m/z (orange) mass channels. The product signal in the 40 m/z channel was determined from conservation of charge because of the mass overlap of this product with the trapped Ca^+ . Delayed growth is observed in the 77 and 79 m/z secondary product channels (combined into one curve displayed in purple). The appearance times, mass-to-charge ratios, and stability of these channels identifies these products as $\text{c-C}_3\text{H}_3^+$ (39 m/z), $\text{C}_2\text{O}^+/\text{C}_3\text{H}_4^+$ (40 m/z), C_6H_5^+ (77 m/z) and C_6H_7^+ (79 m/z). $\text{c-C}_3\text{H}_3^+$, C_2O^+ , and C_3H_4^+ are primary products and the C_6H_y^+ ($y = 5, 7$) ions are secondary products originating from the reaction: $\text{C}_3\text{H}_4^+ + \text{C}_3\text{H}_4$. Ion signals have been normalized to the fitted initial number of O_2^+ ions. Error bars correspond to 1σ standard error. Reproduced from Ref.³⁶ with permission from the Royal Society of Chemistry.

which is comparable in magnitude to the product signal. To reduce the uncertainty arising from the substantial Ca^+ background, we used an indirect method to determine the product ions at $40\text{ }m/z$.

For this indirect method to be valid, two conditions had to be met. First, the total number of ions in the trap needed to remain constant over the course of the reaction. Second, the number of O_2^+ ions loaded into the trap also had to remain consistent, with shot-to-shot variations that were small compared to the average number of O_2^+ ions loaded (~ 180 ions). Once these conditions were satisfied, we determined the number of product ions contributing to the $40\text{ }m/z$ channel using the following equation:

$$N_{40}(t) = N_{\text{O}_2^+}(t = 0) - (N_{\text{O}_2^+}(t) + N_{\text{C}_3\text{H}_3^+}(t) + N_{\text{Secondary Products}}(t)), \quad (3)$$

where $N_{40}(t)$ is the number of ions with a m/z of 40 in the trap at time, t , that are not Ca^+ , $N_{\text{O}_2^+}(t)$ and $N_{\text{C}_3\text{H}_3^+}(t)$ are the number of O_2^+ and C_3H_3^+ ions in the trap at time t , and $N_{\text{Secondary Products}}(t)$ is the number of secondary product ions in the trap at time t that were produced from the reactions of C_3H_4^+ with neutral C_3H_4 .

Although the $40\text{ }m/z$ product could, in principle, have consisted solely of the charge-transfer product C_3H_4^+ , previous studies have shown that C_3H_4^+ reacts with neutral C_3H_4 to form C_6H_5^+ and C_6H_7^+ ,^{34,35} and we observed both reactive and non-reactive — within the timescale of our experiments — components in the $40\text{ }m/z$ channel besides Ca^+ . The secondary products from the $\text{C}_3\text{H}_4^+ + \text{C}_3\text{H}_4$ reaction (77 and $79\text{ }m/z$) accounted for only a small portion of the total product signal ($\sim 3\%$). This suggested most of the ions with $40\text{ }m/z$ were not C_3H_4^+ , and that an additional species was responsible for the non-reacting fraction. Given the atomic composition of the reactants, there were only two possible combinations of atoms that could yield $m/z=40$, C_3H_4^+ and C_2O^+ . Because of this, the most reasonable assignment for the non-reactive $m/z=40$ product was C_2O^+ .

In these previously studied reactions, it appeared that the non-reacting $40\text{ }m/z$ product (likely C_2O^+) accounted for the majority of the $40\text{ }m/z$ product channel. Because these

reactions were conducted with O_2^+ prepared in a mixture of vibrationally excited states, and it is known that vibrational excitations can influence product branching ratios,⁴⁵ we revisited these reactions with O_2^+ prepared in the ground vibrational state to determine how the results of the reaction might be affected by vibrational excitation. The results of these new studies are presented here.

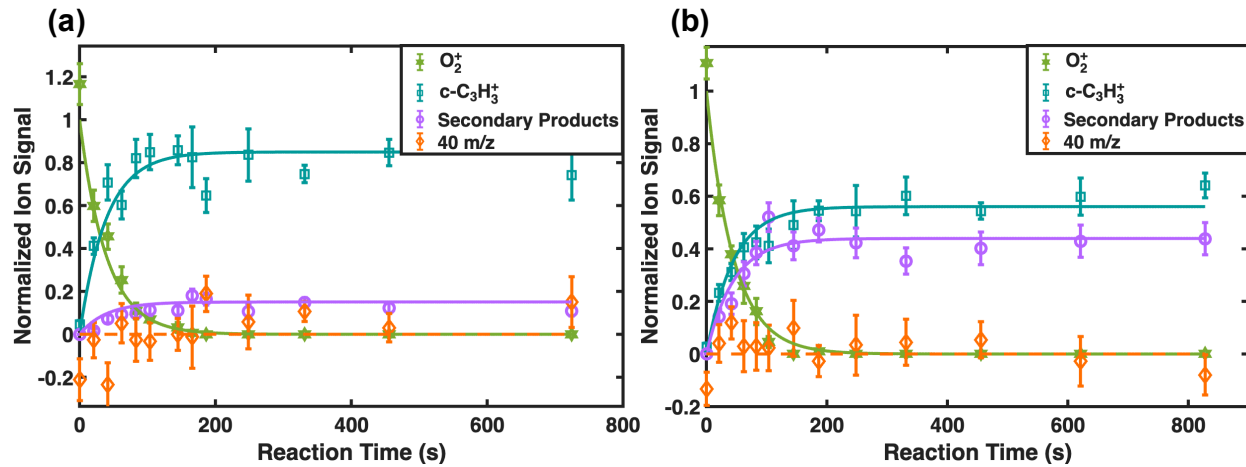


Figure 2: Reaction curves for (a) $O_2^+(v = 0) + H_2C_3H_2$ (allene) and (b) H_3C_3H (propyne) reaction series. As the O_2^+ signal decreases (green), immediate growth is observed in a non-reacting $39\ m/z$ (teal) channel. Because of the mass overlap of a $40\ m/z$ product with the most abundant isotope of Ca^+ , monitoring of this channel had to be carried out by detection of secondary products produced from the reaction: $C_3H_4^+ + C_3H_4$ (combined into one curve displayed in purple). A non-reacting product signal in the $40\ m/z$ channel (orange) was estimated from conservation of charge and revealed to be absent in these ground-state reactions. The appearance times, mass-to-charge ratios, and stability of these channels identifies the products formed in the ground-vibrational state $O_2^+ + C_3H_4$ reactions as $c-C_3H_3^+$ ($39\ m/z$), $C_3H_4^+$, $C_6H_5^+$ ($77\ m/z$) and $C_6H_7^+$ ($79\ m/z$). $c-C_3H_3^+$ and $C_3H_4^+$ are the primary products and the $C_6H_y^+$ ($y = 5, 7$) ions are secondary products. Ion signals have been normalized to the fitted initial number of O_2^+ ions. Error bars correspond to 1σ standard error.

For these studies, we prepared O_2^+ ions in the ground vibrational state and reacted them with both C_3H_4 isomers. Results from these experiments are shown in Fig. 2, where only

two primary products were observed. The majority of product ions from both reactions was the previously observed $c\text{-C}_3\text{H}_3^+$ that accounted for $\sim 85\%$ (~ 60 ions) of all products in the reaction of O_2^+ with allene and $\sim 56\%$ (~ 40 ions) of all products in the reaction of O_2^+ with propyne, see Fig. 2. Unlike the reactions with vibrationally excited O_2^+ , the only other primary product produced was C_3H_4^+ , which accounted for $\sim 15\%$ (~ 10 ions) in the reaction of O_2^+ with allene and $\sim 44\%$ (~ 30 ions) of all products in the reaction of O_2^+ with propyne.

C_3H_4^+ production is determined by measuring the accumulation of products from the $\text{C}_3\text{H}_4^+ + \text{C}_3\text{H}_4$ reaction, which are C_6H_5^+ and C_6H_7^+ . These secondary products can be unambiguously detected in our experiment, with no overlap with Ca^+ or any primary reaction products. If we sum the product ions ($c\text{-C}_3\text{H}_3^+$, C_6H_5^+ , and C_6H_7^+) and remaining reactant ions at any point in time along the reaction curve, we see that the sum is equal to the initial number of reactant O_2^+ ions, as shown in Supplementary Information Figure 1. This conservation demonstrates that, for ground state O_2^+ , no non-reactive $40\text{ }m/z$ products were formed.

This behavior highlights a key distinction between the ground-state and vibrationally excited-state reactions. In the vibrationally excited case, a significant fraction of $40\text{ }m/z$ products did not undergo secondary reactions with C_3H_4 within the time of the experiment, suggesting that two distinct products may have been present in the $40\text{ }m/z$ channel. In contrast, in the ground-state case, all $40\text{ }m/z$ products underwent secondary reactions with C_3H_4 indicating that this product channel consisted exclusively of a single species, C_3H_4^+ . This finding prompted us to confirm the presence of the non-reacting $40\text{ }m/z$ product through a direct measurement.

Although the production of C_2O^+ in the vibrationally excited case was previously suggested from charge conservation arguments,³⁶ we provide additional evidence of the formation of a non-reacting product with $40\text{ }m/z$ here through the use of an isotopically pure $^{44}\text{Ca}^+$ Coulomb crystal and isotopic substitution of the reactants. To remove the large background

signal from $^{40}\text{Ca}^+$ in the mass spectrum, we created an isotopically pure Coulomb crystal of $^{44}\text{Ca}^+$. This was achieved by first preparing a large Coulomb crystal containing approximately 3000 Ca^+ ions with the natural isotopic abundance, and then shifting the cooling-laser frequencies to selectively address the $^{44}\text{Ca}^+$ transitions.^{46,47} The other Ca^+ isotopes left the trap due to heating, either through deliberate parametric excitation for a particular mass or by lowering the trapping potentials to remove high-energy ions. This procedure yielded a small $^{44}\text{Ca}^+$ Coulomb crystal containing approximately 70 ions. While this crystal was sufficiently large to enable product identification, it did not provide enough sympathetic cooling to ensure all product ions remained trapped throughout the full course of a reaction. Consequently, the isotopically purified Coulomb crystal was not used to measure reaction kinetics, but instead served to identify the presence of a non-reacting $40\text{ }m/z$ product.

After preparing the $^{44}\text{Ca}^+$ Coulomb crystal, O_2^+ ions were loaded into the trap in a mixture of vibrationally excited states ($v = 2,3$). Reactions were then performed using either deuterated allene ($\text{D}_2\text{C}_3\text{D}_2$, $m/z=44$) or propyne ($\text{D}_3\text{C}_3\text{D}$, $m/z=44$), which were selected to isolate growth in the $40\text{ }m/z$ channel and thereby support the identification of C_2O^+ as a reaction product.

Growth was observed in the $40\text{ }m/z$ channel in addition to all other expected products ($\text{c-C}_3\text{D}_3^+$ with $m/z=42$ and C_3D_4^+ with $m/z=44$) as shown in Fig. 3. Additional control experiments (e.g., not admitting neutral propyne/allene or not trapping O_2^+) confirmed that the $40\text{ }m/z$ growth originated from reactions between O_2^+ and C_3D_4 and not via reactions with any contaminants. Therefore, because growth in the $40\text{ }m/z$ channel was observed only when both O_2^+ in vibrationally excited states ($v = 2,3$) and C_3X_4 ($\text{X} = \text{H}, \text{D}$) were present, this signal was assigned to the formation of C_2O^+ .

To better understand the origin of C_2O^+ production in *only* the vibrationally excited states, a portion of the potential energy surfaces (PESs) for the reactions between ground-state O_2^+ and the two C_3H_4 isomers were calculated using KinBot to search for barrierless pathways to the observed products.⁴⁸

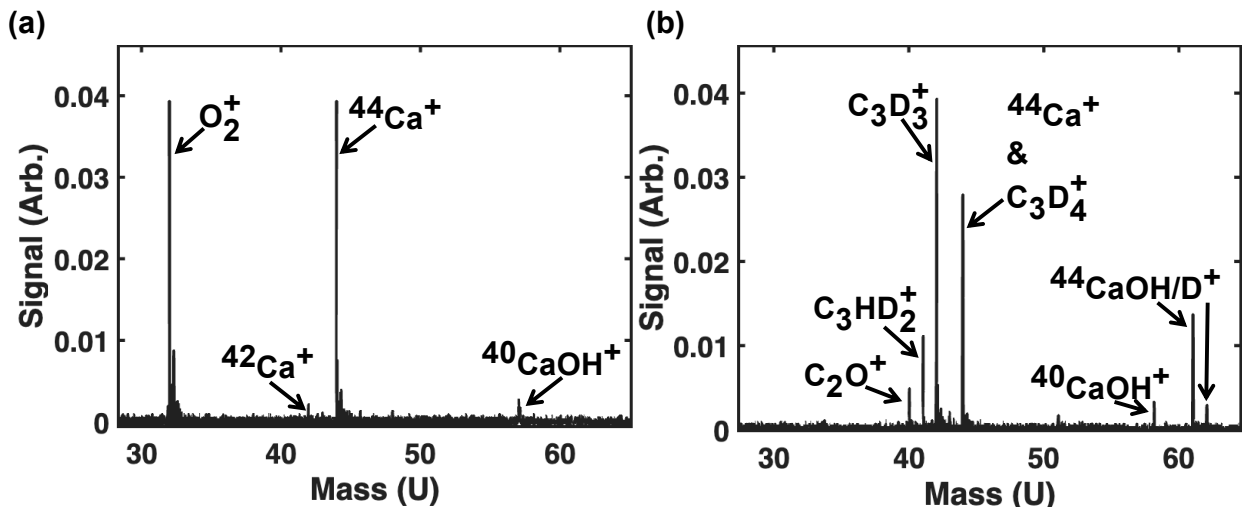


Figure 3: TOF-MS traces depicting the reaction of $O_2^+(v = 2,3) + C_3D_4$ within an isotopically pure $^{44}Ca^+$ Coulomb crystal. These data correspond to a reaction using d4-propyne (D_3C_3D). (a) Example TOF-MS trace at $t = 0$ in which O_2^+ ions are observed at $32\ m/z$ and $^{44}Ca^+$ at $44\ m/z$. The two smaller peaks present correspond to $^{42}Ca^+$ and $^{40}CaOH^+$ ($57\ m/z$). We observe no ions in the $40\ m/z$ location with single ion sensitivity. (b) Example of a TOF-MS trace at $t = 300\ s$ in which O_2^+ has fully reacted with C_3D_4 to form: C_2O^+ at $40\ m/z$, $C_3D_3^+$ at $42\ m/z$, and $C_3D_4^+$ at $44\ m/z$. Additional peaks are also observed at $41\ m/z$ that corresponds to $C_3HD_2^+$, which has formed from H-D swapping between $C_3D_4^+$ and ambient water molecules within the chamber, and at $57\ m/z$, $61\ m/z$ and $62\ m/z$ corresponding to $CaOH^+$ and $CaOD^+$ ions, which are formed from background reactions of Ca^+ with ambient water.

The portion of the PES that shows a possible pathway from reactants to C_2O^+ is shown in Fig. 4 (propyne) and Supporting Information Figure 2 (allene). The energies of the extrema on the surface were zero-point energy corrected and are displayed relative to the reactants' energy at infinite separation. It should be noted that, unlike higher-pressure systems where collisional stabilization can remove energy from the reaction complex, the single-collision conditions employed here preclude such energy loss. As a result, the total energy of the complex remains equal to its initial energy, preventing it from becoming trapped in local minima and allowing it to readily traverse any submerged barriers on the potential energy surface.

The propyne surface begins with a moderately exothermic (1.87 eV) attachment of O_2^+ onto C_3H_4 at INT 1. After this initial attachment, the complex can traverse the surface sampling various orientations of the initial attachment complex before the O–O bond is broken at TS 4. The breaking of the O–O bond and the progression to INT 5 is highly exothermic (~ 4 eV exothermic relative to TS 4). After the O–O bond has been severed, the complex can progress through the surface by a series of low-submerged-barrier proton transfers. These proton transfers result in the complex having rearranged into INT 8, where the complex dissociates into C_2O^+ and the neutral co-product CH_3OH .

The calculated potential energy surfaces revealed that production of C_2O^+ is exothermic and barrierless for the reactions between $\text{O}_2^+(v = 0)$ and both C_3H_4 isomers. KinBot also discovered over 200 energetically allowed product combinations (with 22 unique mass-to-charge ratios), including all of those observed experimentally. Using just thermodynamic arguments with the results of the KinBot calculations, one would conclude that C_2O^+ should be a very minor product as the 127-th lowest-energy product, and other products that we did not detect experimentally, such as C_2H_4^+ and $\text{C}_2\text{H}_3\text{OH}^+$, should have been more prevalent. The observation of C_2O^+ and absence of many products predicted to be more abundant demonstrate that quantum dynamical effects must be at play in these reactions. Such dynamical effects are not uncommon,^{29,51–54} and have been observed to prevent barrierless

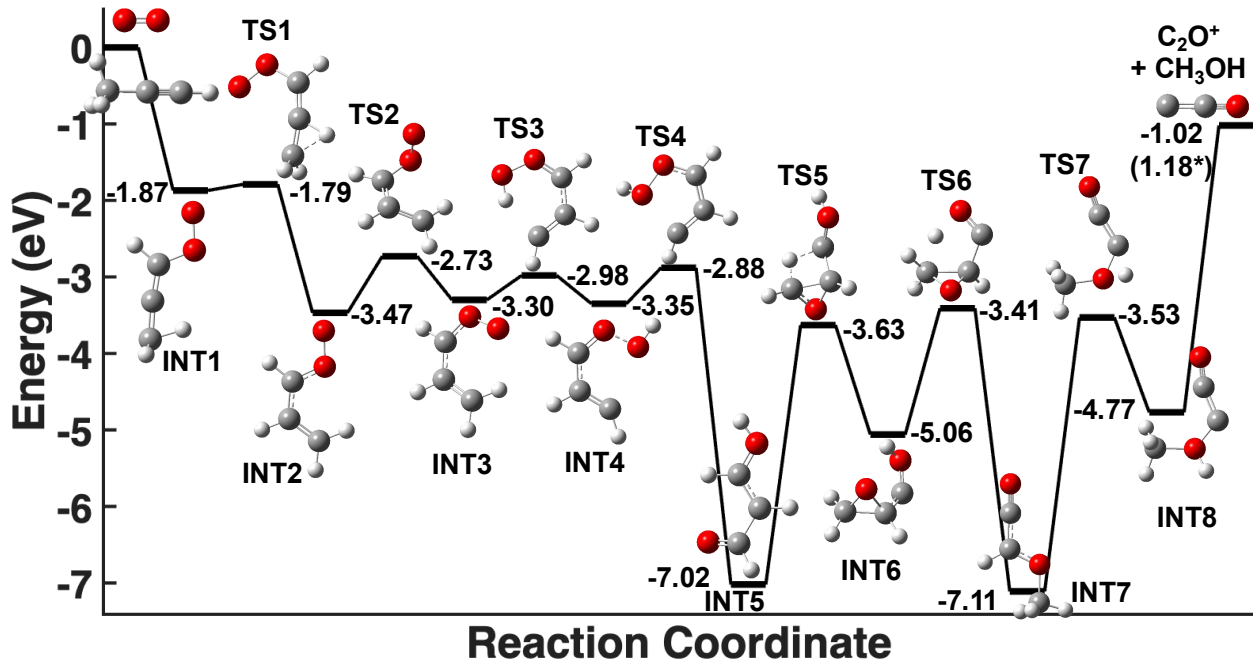


Figure 4: Potential energy surface for the production of C_2O^+ in the reaction between $\text{O}_2^+(v=0)$ and propyne ($\text{H}_3\text{C}_3\text{H}$). All structures were optimized at the MP2/aug-cc-pVTZ level of theory. Single-point energies of these structures were calculated at the CCSD(T)-F12/cc-pVDZ-F12 and have been zero-point energy corrected at the MP2/aug-cc-pVTZ level. All energies are shown relative to reactants energy at infinite separation, with INT1 corresponding to the first stationary point following complex formation. Note that two values are reported for the production of C_2O^+ , one from CCSD(T)-F12 and the asterisked value computed using values from the ATcT database.^{49,50} See Computational Methods for more explanation.

reactions from occurring.^{51,52}

Intuitively, one could argue that production of C_2O^+ was facilitated in the excited-state reactions because the internal reaction coordinate at TS 4 on the C_2O^+ formation PES is directed along the O–O bond. However, for this facilitation to occur, vibrational energy had to remain localized in the O–O bond long enough for this reaction to take place, i.e., until TS 4 is reached. While vibrational energy can, in principle, be removed from a molecule in a variety of ways, including through collision quenching, radiative decay, or intermolecular energy transfer, several of these are unlikely in this particular system. Collisional quenching of excited vibrational modes is not present because of the ultra-high-vacuum environment of the experiment, which leads to single collision conditions. Radiative decay of vibrational excitation occurs on timescales that are not relevant here; neither O_2^+ nor the transient reaction complex has enough time to radiate before the complex dissociates into products. Here, there are two possible modes of energy transfer that could have redistributed the O_2^+ 's initial vibrational energy, a vibration-vibration energy transfer (VVET) during the initial collision and intramolecular vibration redistribution (IVR) during complex formation.

VVET is known to be most efficient when the two colliding partners have vibrational energy spacings that are similar. For example, collisions between vibrationally excited CO_2 and N_2 have been shown to exhibit an order-of-magnitude decrease in energy-transfer efficiency when $^{14}\text{N}_2$ (with an energy mismatch of approximately 18 cm^{-1}) is replaced by $^{15}\text{N}_2$ (with an energy mismatch of approximately 97 cm^{-1}).⁵⁵ For the collisions considered here, the energy of one quanta of the O–O stretch in O_2^+ ($\tilde{\nu} = 1860\text{ cm}^{-1}$, $v = 2\text{-}1$) is substantially mismatched with the nearest energetically accessible vibrational modes of allene ($\text{H}_2\text{C}_3\text{H}_2$) and propyne ($\text{H}_3\text{C}_3\text{H}$), with energy differences of approximately 433 cm^{-1} and 424 cm^{-1} , respectively.^{56–58} Such large energy mismatches make VVET unlikely. Moreover, even if VVET were to occur, the transfer of a single vibrational quantum would not fully quench the excitation of the O–O stretch; instead, multiple sequential quanta would need to be transferred to prevent vibrational energy from remaining localized in the bond during

the initial collision and complex formation.

Although multi-quantum VVET has been observed in systems with high vibrational excitation levels ($v > 15$),⁵⁹ single-quantum transfer processes are nearly an order-of-magnitude more probable for low vibrational excitations ($v < 5$).⁶⁰ Consequently, given that the highest excitation involved in the present reactions was $v = 3$, it is reasonable to conclude that, if VVET occurred at all, it was dominated by single-quantum transfer processes. Thus, following the initial collision between O_2^+ and C_3H_4 , one or two, and potentially even three, vibrational quanta likely remained localized in the O–O stretch. A key question then arises: does this vibrational energy remain localized in the O–O bond during complex formation, or was it rapidly redistributed throughout the reaction complex via IVR?

An estimate for the efficiency of IVR in this reaction can be made based on estimations of the reaction complex's lifetime and typical times associated with IVR. The lifetime of the reaction complex can be roughly approximated through the use of statistical models such as Rice-Ramsperger-Kassel-Marcus (RRKM) theory or transition-state theory.^{61,62} While such calculations assume a thermal distribution of states over the course of the reaction as a result of rapid IVR rates, they can be useful for providing an order-of-magnitude estimate for the complex's lifetime for systems not in thermal equilibrium, as was the case here.

To estimate this lifetime, we performed a simple unimolecular decomposition transition-state theory calculation. In this calculation, the highest energy transition-state structure (TS5, Supporting Information Figure 3) was chosen so as to maximize the complex's estimated lifetime, and the reaction complex's initial structure (INT1, Supporting Information Figure 3) was chosen as the pre-decomposition molecule. These two structures were the only structures used in this calculation. Using these conditions, the calculated lifetime was estimated to be ~ 1 ps. This estimated lifetime is comparable to instances of fast IVR that have been measured to occur over ~ 8 ps;^{63,64} however, it has been found that IVR times typically lie in the 20–90 ps range.^{65–67} The difference in these time ranges suggests that IVR could not occur fully before the complex dissociated into the final products. This implies

that even in the unlikely case that O_2^+ transferred 1 quanta of vibrational energy during the initial collision with C_3H_4 , the leftover vibrational energy remained localized in the O–O stretch, as it would be unable to couple into the complex’s vibrational modes before dissociation occurred. It is reasonable to conclude that this localization facilitated the breaking of the O–O bond at TS 4 (Fig 4) of the calculated potential energy surface and ultimately led to the formation of C_2O^+ . However, this qualitative explanation only rationalizes the observation of C_2O^+ production. This explanation does not clarify why other products that require breaking the O–O bond, such as $\text{C}_2\text{H}_3\text{OH}^+$, are not produced. To understand the full extent of how dynamics influences this particular reaction, one would need to perform quantum dynamics simulations on the complete PES. Such an endeavor is beyond the scope of this work, but we hope our results spur others to explore the dynamics of this complex system.

The results presented here confirm that C_2O^+ is a product in the reactions between $\text{O}_2^+(v = 2,3)$ and C_3H_4 , and demonstrate that the production of C_2O^+ is governed by dynamical effects rather than just by energetics. While we presented qualitative arguments for how these dynamical effects may appear, a more quantitative argument based on quasi-classical trajectories, or other methods, is necessary but would be quite challenging to compute based on the number of atoms involved.

Regardless of the complete details of how dynamics direct the reaction complex to one product over another, it is clear from the experimental data that the pathway to C_2O^+ is effectively activated by vibrational excitation of O_2^+ . The result that preparation of O_2^+ in a vibrationally excited state enables formation of an otherwise unobserved product demonstrates the potential for controlling C_2O^+ production in this reaction. In principle, the branching ratio for C_2O^+ might be further enhanced, possibly to the point of exclusive formation, by preparing O_2^+ in higher vibrational states. Exploration of this possibility, as well as the broader role of O_2^+ vibrational excitation in other reactions, would be well suited to future studies, particularly given the long lifetimes of the excited vibrational states of

O_2^+ . Similar explorations could be made with other homonuclear diatomics and may reveal interesting chemical behaviors and control.

Although full quantum-state control of the $\text{O}_2^+ + \text{C}_3\text{H}_4$ reaction has not yet been realized, this work represents a meaningful advance toward that goal. The results highlight substantial opportunities for probing quantum-state-dependent reactivity and point toward a future in which chemical reaction outcomes can be fully controlled at the quantum level.

Methods

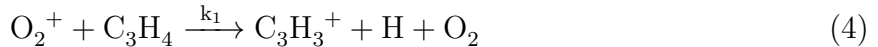
Experimental

Reactions were conducted using our custom-built ion-trapping apparatus, which has been described previously in-depth.⁶⁸ In short, this apparatus consists of a linear, quadrupole ion trap held within an ultra-high-vacuum environment ($\sim 10^{-10}$ Torr). Ca^+ ions were loaded into the trap by non-resonantly photoionizing (~ 7 mJ/pulse, 355 nm, 10 Hz) an effusive source of Ca in the center of the ion trap. These trapped Ca^+ ions were then laser cooled to sub-Kelvin temperatures using the doubled output of a Ti-Sapph laser (~ 397 nm, 2 mW) and a diode laser (~ 866 nm, 2 mW). O_2^+ ions were then co-trapped with the Ca^+ ions by resonantly photoionizing a supersonic molecular beam of O_2 in He (2% mixture) in the center of the trap. Two (2 + 1) REMPI schemes at ~ 301 nm and ~ 288 nm were used to form O_2^+ ions predominantly in the ground or vibrationally excited states ($v = 2,3$), respectively.^{37–40}

The O_2^+ ions were then sympathetically cooled by the laser-cooled Ca^+ ions to secular temperatures ~ 1 K. As the ions cooled, they self-arranged into a pseudo-crystalline structure known as a Coulomb crystal. Within the Coulomb crystal, the spacing between ions is around $\sim 10 \mu\text{m}$ due to the Coulomb repulsion. Consequently, only the translational motion is sympathetically cooled, while the vibrational and rotational state populations remain unperturbed by the co-trapped ions.

After the O_2^+ ions had been trapped and cooled, reactions were initiated by admitting

either neutral allene ($\text{H}_2\text{C}_3\text{H}_2$) or propyne ($\text{H}_3\text{C}_3\text{H}$) into the chamber through a pulsed leak valve at a constant pressure ($\sim 1.2 \times 10^{-9}$ Torr for the ground-state reactions and $\sim 0.3 \times 10^{-9}$ Torr for the excited-state reactions) for variable periods of time (0 – 350 seconds). At various reaction times, the contents of the trap were ejected into a time-of-flight mass spectrometer (TOF-MS) to measure the number of ions at each m/z . A new Coulomb crystal was loaded for each measurement. Measurements at each time point were repeated > 7 times, and the mean and standard error of the mean were plotted and globally fit, with the following chemical equations and pseudo-first order rate equations (where allene and propyne are treated in excess), as a function of reaction time to produce the observed reaction curves.



$$\frac{d(\text{O}_2^+)}{dt} = -(k_1 + k_2) \times \text{O}_2^+(t) \quad (6)$$

$$\frac{d(\text{C}_3\text{H}_3^+)}{dt} = k_1 \times \text{O}_2^+(t) \quad (7)$$

$$\frac{d(\text{C}_3\text{H}_4^+ + \text{Secondary Products})}{dt} = k_2 \times \text{O}_2^+(t) \quad (8)$$

Where k_1 and k_2 correspond to fitted pseudo-first order rate constants for production of C_3H_3^+ and C_3H_4^+ , respectively, and are reported in Supplementary Information Table 1. As C_3H_4^+ shares a mass channel with the most abundant isotope of Ca^+ , direct observation of C_3H_4^+ resulted in large uncertainties from the fitting routine originating from fluctuations in Ca^+ loading. These fluctuations from Ca^+ (± 50 ions) were avoided by indirectly monitoring the C_3H_4^+ product channel by instead fitting to the directly observed growth of secondary products from the reactions of C_3H_4^+ with additional neutral C_3H_4 molecules (with total fluctuations of ~ 5 ions). While this approximation does not capture the short reaction time behavior of C_3H_4^+ , it captured the C_3H_4^+ branching in the long reaction time limit.

Computational Methods

Our goal in this work was to identify feasible pathways to the observed products and not to provide a complete and accurate kinetic characterization of the processes at play, especially given the experimental results that suggest dynamics dominate the branching between the open channels.

To identify feasible pathways, potential energy surfaces (PES) for the reaction between O_2^+ ($v = 0$) and the C_3H_4 isomers were explored using KinBot to search for barrierless (i.e., submerged relative to the reactants) pathways to products. KinBot has been described in-depth previously,^{48,69} and only a brief description is provided here. KinBot is an open-source chemical kinetics workflow code that can explore and characterize reactive potential energy surfaces typically with the aim to predict reaction rate constants. KinBot calculations begin with a geometry optimization of a specified ‘reactant’ molecule, which in this study is the $[\text{O}_2-\text{C}_3\text{H}_4]^+$ reaction complex. After this optimization, KinBot generates saddle point guess structures by systematically modifying the initial geometry via a series of constrained optimizations as dictated by reaction templates. These guess structures are then optimized to true saddle points, and, if the optimization is successful and the structure’s energy is below a user-defined threshold, intrinsic reaction coordinate (IRC) calculations are used to ensure the connectivity of the saddle to the reactant and to identify the product(s). If the reaction product is an isomer of the original well, a new exploration is started by the code until all connected and valid wells are found.

KinBot uses various levels of theory in its workflow. The exploration phase is typically done at a low level of theory, which was L1 = UB3LYP/6-31+G(d) in this work. Then, the structures are refined at a higher level of theory to obtain better geometries and rovibrational properties, L2. Finally, if desired, the energies can be further refined using single-point energy corrections, L3. For L2 and L3, we used various methods to better understand the underlying uncertainties for the reaction paths of interest. The reported energies (shown in Supplementary Information Tables 2 and 3) are at UMP2/aug-cc-pVTZ, ω B97X-D/6-311++G(d,p),

and CCSD(T)-F12a/cc-pVDZ-F12//UMP2/aug-cc-pVTZ levels of theory. All intermediates and transition states were assumed to be doublets on the $\text{C}_3\text{H}_4\text{O}_2^+$ PES. O_2^+ is assigned D_{2h} symmetry in Molpro 2023,⁷⁰ which can use only Abelian point groups. The ground state of O_2^+ is $^2\Pi_g$, which translates into B_{2g} or B_{3g} in Molpro. The calculated energies for these two states are degenerate, in line with the underlying D_{2h} symmetry. C_2O^+ is also linear but not centrosymmetric (its connectivity is C-C-O), therefore, its Abelian group is C_{2v} . The ground state of C_2O^+ is the $^2\Pi$ state,⁷¹ correlating with the degenerate (for this system) B_1 and B_2 symmetries. However, unlike for O_2^+ , the CCSD(T)-F12 method yields two non-degenerate states, of which we report the lower one. A more accurate calculation would involve a multi-reference method instead of the single-reference CCSD(T)-F12 method, which further requires careful choices of other species for proper referencing of relative energies. To reduce some of the uncertainties introduced by the single-reference method for C_2O^+ we report both a CCSD(T)-F12 energy and a value determined using the ATcT v.1.220 database for comparison.^{49,50} For the DFT and MP2 calculations we used Gaussian 16,⁷² while for the CCSD(T)-F12 energies we used Molpro.

Using the above workflow, we were able to determine an expansive potential energy surface for this reaction. We found a very large number of pathways, with >150 wells and >200 bimolecular product channels at L1, all satisfying the energetic criterion, which was that no barrier shall be above the energy of the starting species. The reason for the vastness of the PES is that the reactants initially form very strong bonds at the addition step. After this attachment, the PES descends rapidly by breaking the O–O bond, resulting in several wells on the PES that are 6 eV or deeper relative to the reactants. We analyzed the large reaction network using our postprocessing tool, PESViewer,⁷³ which allowed us to find feasible pathways between any two species on the surface and explore some pathways manually.

Acknowledgement

The authors thank Alicja Karpinska for her contributions to data acquisition. This work was supported by the National Science Foundation (PHY-2317149) and the Air Force Office of Scientific Research (FA9550-16-1-0117). J.Z. is supported by the U.S. Department of Energy (DOE), Office of Science, Office of Basic Energy Sciences, Division of Chemical Sciences, Geosciences and Biosciences via the Gas Phase Chemical Physics program. This article has been authored by employees of National Technology and Engineering Solutions of Sandia, LLC, under Contract No. DE-NA0003525 with the U.S. DOE. The employees co-own right, title, and interest in and to the article and are responsible for its contents. The United States Government retains and the publisher, by accepting the article for publication, acknowledges that the United States Government retains a nonexclusive, paid-up, irrevocable, worldwide license to publish or reproduce the published form of this article or allow others to do so, for United States Government purposes. The DOE will provide public access to these results of federally sponsored research in accordance with the DOE Public Access Plan <https://www.osti.gov/public-access>.

Supporting Information Available

Includes additional potential energy surfaces, a table of fitted rate constants, and tables of additional thermochemical calculations (PDF)

References

(1) Chen, Q.; Zhang, S.; Hu, X.; Xie, D.; Guo, H. Reaction Pathway Control via Reactant Vibrational Excitation and Impact on Product Vibrational Distributions: The O +

$\text{HO}_2 \rightarrow \text{OH} + \text{O}_2$ Atmospheric Reaction. *J. Phys. Chem. Lett.* **2022**, *13*, 1872–1878.

(2) Polanyi, J. C. Some Concepts in Reaction Dynamics. *Acc. Chem. Res.* **1972**, *5*, 161–168.

(3) Anlauf, K. G.; Maylotte, D. H.; Polanyi, J. C.; Bernstein, R. B. Rates of the Endothermic Reactions $\text{HCl} + \text{X}(\text{X} \equiv \text{I}, \text{Cl})$ as a Function of Reagent Vibration, Rotation, and Translation. *J. Chem. Phys.* **1969**, *51*, 5716–5717.

(4) Polanyi, J. C.; Tardy, D. C. Energy Distribution in the Exothermic Reaction $\text{F} + \text{H}_2$ and the Endothermic Reaction $\text{HF} + \text{H}$. *J. Chem. Phys.* **1969**, *51*, 5717–5719.

(5) Parker, J. H.; Pimentel, G. C. Vibrational Energy Distribution Through Chemical Laser Studies. I. Fluorine Atoms Plus Hydrogen or Methane. *J. Chem. Phys.* **1969**, *51*, 91–96.

(6) Moore, C. B.; Smith, I. W. M. Vibrational-Rotational Excitation. Chemical Reactions of Vibrationally Excited Molecules. *Faraday Discuss. Chem. Soc.* **1979**, *67*, 146–161.

(7) Honma, K.; Tanaka, K.; Koyano, I.; Tanaka, I. The Effect of Vibrational and Translational Energies of Ionic Reactant on the Reaction $\text{NO}^+ + \text{iso-C}_4\text{H}_{10} \rightarrow \text{HNO} + \text{C}_4\text{H}_9^+$. *J. Chem. Phys.* **1976**, *65*, 678–683.

(8) Honma, K.; Tanaka, I. Effect of Vibrational and Translational Energies of C_2H_2^+ on the Reaction with Methane. *J. Chem. Phys.* **1979**, *70*, 1893–1897.

(9) Yang, B.; Chiu, Y.-H.; Anderson, S. L. The Effects of Reactant Vibrational, Fine Structure, and Collision Energy on the Reactions of OCS^+ with C_2H_2 : Complementary Studies of Reactions in the $[\text{C}_2\text{H}_2 + \text{OCS}]^+$ System. *J. Chem. Phys.* **1991**, *94*, 6459–6468.

(10) Yan, S.; Wu, Y.-T.; Zhang, B.; Yue, X.-F.; Liu, K. Do Vibrational Excitations of CHD_3 Preferentially Promote Reactivity Toward the Chlorine Atom? *Science* **2007**, *316*, 1723–1726.

(11) Dotan, I.; Viggiano, A. A. Kinetics of the Reaction of O_2^+ with CH_4 from 500 to 1400 K: A Case for State Specific Chemistry. *J. Chem. Phys.* **2001**, *114*, 6112–6118.

(12) Ellerbrock, R.; Zhao, B.; Manthe, U. Vibrational Control of the Reaction Pathway in the $H + CHD_3 \rightarrow H_2 + CD_3$ Reaction. *Sci. Adv.* **2022**, *8*.

(13) Jiang, B.; Guo, H. Relative Efficacy of Vibrational vs. Translational Excitation in Promoting Atom-Diatom Reactivity: Rigorous Examination of Polanyi's Rules and Proposition of Sudden Vector Projection (SVP) Model. *J. Chem. Phys.* **2013**, *138*.

(14) Papp, D.; Li, J.; Guo, H.; Czakó, G. Vibrational Mode-Specificity in the Dynamics of the $Cl + C_2H_6 \rightarrow HCl + C_2H_5$ Reaction. *J. Chem. Phys.* **2021**, *155*, 114303.

(15) Zanchet, A.; Agúndez, M.; Herrero, V. J.; Aguado, A.; Roncero, O. Sulfur Chemistry in the Interstellar Medium: The Effect of Vibrational Excitation of H_2 in the Reaction $S^+ + H_2 \rightarrow SH^+ + H$. *AJ* **2013**, *146*.

(16) Wang, C.; Liu, S.; Zhang, D. H. Effects of Reagent Vibrational Excitation on the State-to-State Quantum Dynamics of the $OH + CO \rightarrow H + CO_2$ Reaction in Six Dimensions ($J = 0$). *Chem. Phys. Letters* **2012**, *537*, 16–20.

(17) Song, H.; Li, A.; Guo, H. Rotational and Isotopic Effects in the $H_2 + OH^+ \rightarrow H + H_2O^+$ Reaction. *J. Phys. Chem. A* **2016**, *120*, 4742–4748.

(18) Glowacki, D. R.; Lockhart, J.; Blitz, M. A.; Klippenstein, S. J.; Pilling, M. J.; Robertson, S. H.; Seakins, P. W. Interception of Excited Vibrational Quantum States by O_2 in Atmospheric Association Reactions. *Science* **2012**, *337*, 1066–1069.

(19) Csorba, B.; Szabó, P.; Góger, S.; Lendvay, G. The Role of Zero-Point Vibration and Reactant Attraction in Exothermic Bimolecular Reactions with Submerged Potential Barriers: Theoretical Studies of the $R + HBr \rightarrow RH + Br$ ($R = CH_3, HO$) Systems. *J. Phys. Chem. A* **2021**, *125*, 8386–8396.

(20) Viggiano, A. A.; Morris, R. A. Rotational and Vibrational Energy Effects on Ion-Molecule Reactivity as Studied by the VT-SIFDT Technique. *J. Phys. Chem.* **1996**, *100*, 19227–19240.

(21) Agúndez, M.; Goicoechea, J. R.; Cernicharo, J.; Faure, A.; Roueff, E. The Chemistry of Vibrationally Excited H₂ in the Interstellar Medium. *ApJ* **2010**, *713*, 662–670.

(22) Xu, Y.; Xiong, B.; Chang, Y. C.; Ng, C. Y. The Translational, Rotational, and Vibrational Energy Effects on the Chemical Reactivity of Water Cation H₂O⁺(X²B₁) in the Collision with Deuterium Molecule D₂. *J. Chem. Phys.* **2013**, *139*, 024203.

(23) Markus, C. R.; Asvany, O.; Salomon, T.; Schmid, P. C.; Brünken, S.; Lipparini, F.; Gauss, J.; Schlemmer, S. Vibrational Excitation Hindering an Ion-Molecule Reaction: The c-C₃H₂⁺ – H₂ Collision Complex. *Phys. Rev. Lett.* **2020**, *124*, 233401.

(24) Crim, F. F. Chemical Dynamics of Vibrationally Excited Molecules: Controlling Reactions in Gases and on Surfaces. *PNAS* **2008**, *105*, 12654–12661.

(25) Green, R. J.; Kim, H.-T.; Qian, J.; Anderson, S. L. Complex Formation, Rearrangement, and Reaction in PhOH⁺ + ND₃: Vibrational Mode Effects, Recoil Velocities, and *ab initio* Studies. *J. Chem. Phys.* **2000**, *113*, 4158–4170.

(26) Hahn, R.; Schlander, D.; Zhelyazkova, V.; Merkt, F. Opposite Effects of the Rotational and Translational Energy on the Rates of Ion-Molecule Reactions Near 0 K: The D₂⁺ + NH₃ and D₂⁺ + ND₃ Reactions. *Phys. Rev. X* **2024**, *14*, 011034.

(27) Venkataramanababu, S.; Li, A.; Antonov, I. O.; Dragan, J. B.; Stollenwerk, P. R.; Guo, H.; Odom, B. C. Enhancing Reactivity of SiO⁺ Ions by Controlled Excitation to Extreme Rotational States. *Nat Commun.* **2023**, *14*.

(28) Puri, P.; Mills, M.; Schneider, C.; Simbotin, I.; Montgomery, J. A.; Côté, R.;

Suits, A. G.; Hudson, E. R. Synthesis of Mixed Hypermetallic Oxide BaOCa^+ from Laser-Cooled Reagents in an Atom-Ion Hybrid Trap. *Science* **2017**, *357*, 1370–1375.

(29) Yang, T.; Li, A.; Chen, G. K.; Xie, C.; Suits, A. G.; Campbell, W. C.; Guo, H.; Hudson, E. R. Optical Control of Reactions between Water and Laser-Cooled Be^+ Ions. *J. Phys. Chem. Lett.* **2018**, *9*, 3555–3560.

(30) Armentrout, P. B. Fundamentals of Ion-Molecule Chemistry. *J. Anal. At. Spectrom.* **2004**, *19*, 571–580.

(31) Peek, J. M.; Hashemi-Attar, A.-R.; Beckel, C. L. Spontaneous Emission Lifetimes in the Ground Electronic States of HD^+ and H_2^+ . *J. Chem. Phys.* **1979**, *71*, 5382–5383.

(32) Salloum, A.; Dubost, H. Vibrational Energy Transfer from CO to O_2 in Rare Gas Matrices. I. Vibrational Excitation and Relaxation of O_2 (X, $v = 4 - 20$). *Chem. Phys.* **1994**, *189*, 179–204.

(33) Wetmore, R. W.; Fox, J. L.; Dalgarno, A. Radiative Lifetimes of the Second Negative System of O_2^+ . *Planet. Space Sci.* **1984**, *32*, 1111–1113.

(34) Schmid, P. C.; Greenberg, J.; Nguyen, T. L.; Thorpe, J. H.; Catani, K. J.; Krohn, O. A.; Miller, M. I.; Stanton, J. F.; Lewandowski, H. J. Isomer-Selected Ion-Molecule Reactions of Acetylene Cations with Propyne and Allene. *Phys. Chem. Chem. Phys.* **2020**, *22*, 20303–20310.

(35) Greenberg, J.; Schmid, P. C.; Thorpe, J. H.; Nguyen, T. L.; Catani, K. J.; Krohn, O. A.; Miller, M. I.; Stanton, J. F.; Lewandowski, H. J. Using Isotopologues to Probe the Potential Energy Surface of Reactions of $\text{C}_2\text{H}_2^+ + \text{C}_3\text{H}_4$. *J. Chem. Phys.* **2021**, *154*, 124310.

(36) Zagorec-Marks, C.; Kocheril, G. S.; Krohn, O. A.; Kieft, T.; Karpinska, A.; Softley, T. P.; Lewandowski, H. J. To Form or not to Form a Reaction Complex: Exploring

Ion-Molecule Reactions Between C_3H_4 Isomers and Xe^+ and O_2^+ . *Faraday Discuss.* **2024**, *251*, 125–139.

(37) Singh, A. P.; Mitchell, M.; Henshon, W.; Hartman, A.; Lunstad, A.; Kuzhan, B.; Hanneke, D. State Selective Preparation and Nondestructive Detection of Trapped O_2^+ . *J. Chem. Phys.* **2025**, *162*, 054203.

(38) Katsumata, S.; Sato, K.; Achiba, Y.; Kimura, K. Excited-State Photoelectron Spectra of the One-Photon Forbidden $C^3\Pi_g$ Rydberg State of Molecular Oxygen. *J. Electron Spectry.* **1986**, *41*, 325–335.

(39) Stephens, J. A.; Braunstein, M.; McKoy, V.; Rudolph, H.; Lee, M. T. Non-Franck-Condon Effects Induced by Shape Resonances and Orbital Evolution in Resonance Enhanced Multiphoton Ionization of Small Molecules. *Phys. Scr.* **1990**, *41*, 482.

(40) Wu, Y.; Zhang, Z.; Adams, S. F. O_2 Rotational Temperature Measurements by Coherent Microwave Scattering from REMPI. *Chem. Phys. Letters* **2011**, *513*, 191–194.

(41) McEwan, M. J.; McConnell, C. L.; Freeman, C. G.; Anicich, V. G. Reactions of Isomeric $C_3H_3^+$ Ions: A Combined Low Pressure-High Pressure Study. *J. Phys. Chem.* **1994**, *98*, 5068–5073.

(42) Ausloos, P. J.; Lias, S. G. Discrimination of $C_3H_3^+$ Structures on the Basis of Chemical Reactivity. *J. Am. Chem. Soc.* **1981**, *103*, 6505–6507.

(43) Gupta, D.; Schmid, P. C.; Salomon, T.; Asvany, O.; Schlemmer, S. Rotationally Resolved Spectrum of the Degenerate Antisymmetric C-H Stretching Band of c- $C_3H_3^+$. *ACS Earth Space Chem.* **2025**, *9*, 952–958.

(44) Zhao, D.; Doney, K. D.; Linnartz, H. Laboratory Gas-Phase Detection of the Cyclopropenyl Cation (c- $C_3H_3^+$). *ApJL* **2014**, *791*, L28.

(45) Liu, J.; Anderson, S. L. Dynamical Control of ‘Statistical’ Ion-Molecule Reactions. *Int. J. of Mass Spectrom.* **2005**, *241*, 173–184.

(46) Hashimoto, Y.; Nagamoto, D.; Hasegawa, S. Isotope Selective Manipulation and Observation of Ca^+ Ions by Ion Trap-Laser Cooling Technique. *Int. J. of Mass Spectrom.* **2009**, *279*, 163–169.

(47) Mårtensson-Pendrill, A.-M.; Ynnerman, A.; Warston, H.; Vermeeren, L.; Silverans, R. E.; Klein, A.; Neugart, R.; Schulz, C.; Lievens, P.; Collaboration, T. I. Isotope Shifts and Nuclear-Charge Radii in Singly Ionized $^{40-48}\text{Ca}$. *Phys. Rev. A* **1992**, *45*, 4675.

(48) Van de Vijver, R.; Zádor, J. KinBot: Automated Stationary Point Search on Potential Energy Surfaces. *Comput. Phys. Commun.* **2020**, *248*, 106947.

(49) Ruscic, B.; Pinzon, R. E.; Morton, M. L.; von Laszewski, G.; Bittner, S. J.; Nijssure, S. G.; Amin, K. A.; Minkoff, M.; Wagner, A. F. Introduction to Active Thermochemical Tables: Several “Key” Enthalpies of Formation Revisited. *J. Phys. Chem. A* **2004**, *108*, 9979–9997.

(50) Ruscic, B.; Pinzon, R. E.; von Laszewski, G.; Kodeboyina, D.; Burcat, A.; Leahy, D.; Montoy, D.; Wagner, A. F. Active Thermochemical Tables: Thermochemistry for the 21st Century. *J. Phys.: Conf. Ser.* **2005**, *16*, 561–570.

(51) Li, A.; Li, Y.; Guo, H.; Lau, K.-C.; Xu, Y.; Xiong, B.; Chang, Y.-C.; Ng, C. Y. Communication: The Origin of Rotational Enhancement Effect for the Reaction of $\text{H}_2\text{O}^+ + \text{H}_2$ (D_2). *J. Chem. Phys.* **2014**, *140*, 011102.

(52) Kocheril, G. S.; Zagorec-Marks, C.; Lewandowski, H. J. Termination of Bottom-Up Interstellar Aromatic Ring Formation at C_6H_5^+ . *Nat Astron* **2025**, *9*, 685–691.

(53) Carrascosa, E.; Meyer, J.; Wester, R. Imaging the Dynamics of Ion–Molecule Reactions. *Chem. Soc. Rev.* **2017**, *46*, 7498–7516.

(54) Lu, X.; Shang, C.; Li, L.; Chen, R.; Fu, B.; Xu, X.; Zhang, D. H. Unexpected Steric Hindrance Failure in the Gas Phase $\text{F} + (\text{CH}_3)_3\text{Cl}$ SN2 Reaction. *Nat Commun.* **2022**, *13*.

(55) Sharma, R. D.; Brau, C. A. Energy Transfer in Near-Resonant Molecular Collisions due to Long-Range Forces with Application to Transfer of Vibrational Energy from ν_3 Mode of CO_2 to N_2 . *J. Chem. Phys.* **1969**, *50*, 924–930.

(56) Shamir, J.; Binenboym, J.; Claassen, H. H. The Vibrational Frequency of the Oxygen Molecule (O_2^+) Cation. *J. Am. Chem. Soc.* **1968**, *90*, 6223–6224.

(57) Es-sebbar, E.; Jolly, A.; Benilan, Y.; Farooq, A. Quantitative Mid-Infrared Spectra of Allene and Propyne from Room to High Temperatures. *J. Mol. Spectrosc.* **2014**, *305*, 10–16.

(58) Shimanouchi, T. *Tables of Molecular Vibrational Frequencies Consolidated Volume I*; National Bureau of Standards, 1972; pp 1–160.

(59) Mack, J. A.; Mikulecky, K.; Wodtke, A. M. Resonant Vibration-Vibration Energy Transfer Between Highly Vibrationally Excited $\text{O}_2(X^3\Sigma_g^-$, $v=15\text{--}26$) and CO_2 , N_2O , N_2 , and O_3 . *J. Chem. Phys.* **1996**, *105*, 4105–4116.

(60) Chen, J.; Li, J.; Bowman, J. M.; Guo, H. Energy Transfer Between Vibrationally Excited Carbon Monoxide Based on a Highly Accurate Six-Dimensional Potential Energy Surface. *J. Chem. Phys.* **2020**, *153*, 054310.

(61) Croft, J. F. E.; Bohn, J. L. Long-Lived Complexes and Chaos in Ultracold Molecular Collisions. *Phys. Rev. A* **2014**, *89*, 012714.

(62) Carroll, J. J.; Haug, K. L.; Weisshaar, J. C.; Blomberg, M. R. A.; Siegbahn, P. E. M.; Svensson, M. Gas Phase Reactions of Second-Row Transition Metal Atoms with Small Hydrocarbons: Experiment and Theory. *J. Phys. Chem.* **1995**, *99*, 13955–13969.

(63) Charvat, A.; Aßmann, J.; Abel, B.; Schwarzer, D. Real-Time Probing of Intramolecular Vibrational Energy Redistribution and Intermolecular Vibrational Energy Transfer of Selectively Excited CH_2I_2 Molecules in Solution. *J. Phys. Chem. A* **2001**, *105*, 5071–5080.

(64) Elles, C. G.; Cox, M. J.; Crim, F. F. Vibrational Relaxation of CH_3I in the Gas Phase and in Solution. *J. Chem. Phys.* **2004**, *120*, 6973–6979.

(65) Yamada, Y.; Okano, J.; Mikami, N.; Ebata, T. Picosecond IR-UV Pump-Probe Spectroscopic Study on the Intramolecular Vibrational Energy Redistribution of NH_2 and CH Stretching Vibrations of Jet-Cooled Aniline. *J. Chem. Phys.* **2005**, *123*, 124316.

(66) Cao, L.; Wang, Y.; Lu, X.; Zhang, S. Investigation on the Vibrational Relaxation and Ultrafast Electronic Dynamics of S_1 State in 2,4-Difluoroanisole. *J. Chem. Phys.* **2024**, *161*, 124307.

(67) Yoo, H. S.; McWhorter, D. A.; Pate, B. H. Vibrational Dynamics of Terminal Acetylenes: III. Comparison of the Acetylenic C-H Stretch Intramolecular Vibrational-Energy Redistribution Rates in Ultracold Molecular Beams, Room-Temperature Gases, and Room-Temperature Dilute Solutions. *J. Phys. Chem. A* **2004**, *108*, 1380–1387.

(68) Schmid, P. C.; Greenberg, J.; Miller, M. I.; Loeffler, K.; Lewandowski, H. J. An Ion Trap Time-of-Flight Mass Spectrometer with High Mass Resolution for Cold Trapped Ion Experiments. *Rev. Sci. Instrum.* **2017**, *88*, 123107.

(69) Zádor, J.; Martí, C.; Van de Vijver, R.; Johansen, S. L.; Yang, Y.; Michelsen, H. A.; Najm, H. N. Automated Reaction Kinetics of Gas-Phase Organic Species over Multiwell Potential Energy Surfaces. *J. Phys. Chem. A* **2023**, *127*, 565–588.

(70) Werner, H.-J.; Knowles, P. J.; Celani, P.; Győrffy, W.; Hesselmann, A.; Kats, D.; Knizia, G.; Köhn, A.; Korona, T.; Kreplin, D. et al. Molpro, version 2023.2, a package of ab initio programs. 2023; <https://www.molpro.net>, see <https://www.molpro.net>.

(71) Jutier, L.; Léonard, C. *Ab initio* study of the C₂O⁺ cation. *Mol. Phys.* **2007**, *105*, 1105–1114.

(72) Frisch, M. J.; Trucks, G. W.; Schlegel, H. B.; Scuseria, G. E.; Robb, M. A.; Cheeseman, J. R.; Scalmani, G.; Barone, V.; Petersson, G. A.; Nakatsuji, H. et al. Gaussian¹⁶ Revision C.01. 2016; Gaussian Inc. Wallingford CT.

(73) Van de Vijver, R.; Martí, C.; Zádor, J. PESViewer. <https://github.com/rubenvdvijver/PESViewer>, 2023.